NEUTRON CROSS SECTION DATA LIBRARY FOR PD-105, AG-109, XE-131 AND CS-133

Y. D. LEE and J. H. CHANG
Korea Atomic Energy Research Institute
P.O. Box105, Yuseong, Daejeon, Korea 305-600
Tel: 042-868-2635, FAX: 042-868-2636
E-mail : ydlee@kaeri.re.kr

The neutron induced nuclear cross-section data for Pd-105, Ag-109, Xe-131, and Cs-133 were calculated and evaluated from an unresolved energy to 20 MeV. The energy dependent optical model potential parameters were extracted based on recent experimental data and applied up to 20 MeV. A spherical optical model and a statistical model for the equilibrium energy, and a multistep direct and a multistep compound model for the pre-equilibrium energy were used in the calculation. The direct capture model was recently introduced for fast neutron capture. The theoretically calculated cross-sections were compared with the experimental data and the evaluated files. The total and capture cross-sections calculated using the model were in good agreement with the reference experimental data. The evaluated cross-section results were compiled in ENDF-6 format and merged with the resonance component, already adopted in the ENDF/B-VI release 8. New data library files covering from thermal to 20 MeV were created. They are at the preliminary stage of an ENDF/B-VII release.

KEYWORDS : neutron, cross section, evaluation, fission products, data library

1. INTRODUCTION

Neutron cross-section data evaluation for fission products that mainly influence the reactivity in a fission reactor has been performed under a joint project with the National Nuclear Data Center (NNDC) of the Brookhaven National Laboratory (BNL). The results for other nuclei among the selected fission products was made into a full data library by merging them with the resonance part and those already published elsewhere [1,2]. The current evaluation is basically divided into two categories: the thermal to resonance region and the upper resonance region up to 20 MeV. A different theory and procedure are applied to each energy region for the cross-section calculation. For the resonance energy region, the evaluation was already conducted for all the selected nuclei and the results were adopted in the ENDF/B-VI release 8 up to an unresolved energy region [3]. In this paper, the cross-section calculation and evaluation results are presented on Pd-105, Ag-109, Xe-131, and Cs-133 from an unresolved energy up to 20 MeV, for (n, tot), (n, n), (n, n'), (n, γ), and (n, p) reaction. The current evaluation results will complement the evaluation of the resonance region.

Neutron induced nuclear reaction data for fission products are important for predicting burn-up performance in a fission reactor, criticality for spent fuel storage design, advanced fuel performance, and radiation damage estimation of structural material. Neutron capture cross-sections of fission products in several keV regions are significant in a fission reactor with respect to neutron absorption loss. The absorbed neutrons by fission products constitute a large portion of the total loss of neutrons in a reactor.

Pd-105, Ag-109, Xe-131, and Cs-133 are stable isotopes and have 22.33 %, 48.16 %, 21.2 %, and 100 % natural elemental abundance, respectively. They are produced in a nuclear reactor by fission, but are mainly accumulated from beta decay and electron capture from their parent nuclides. ENDF/B-VI on Pd-105 was modified by P.G. Young (Los Alamos National Lab) for the fast energy region in 1996. Below 1 keV, the calculations were matched to the resonance parameters (ENDF/B-VI). For incident and exiting neutrons, a phenomenological optical model potential by Arthur and Young [4] was utilized and corrections for direct reactions were made. For Ag-109, Xe-131, and Cs-133, ENDF/V evaluations were conducted in 1983, 1978, and 1978, respectively. They were converted to ENDF-6 format by the National Nuclear Data Center in 1990 and formed for the ENDF/B-VI in the fast energy region.

The evaluation consists of an optical model potential search followed by a complete nuclear reaction model calculation and validation for the experimental data. The optical model potential depending on the incident neutron energy is searched using a graphical interface [5] of ABA-REX [6]. The potential form and corresponding parameters are selected by comparing the model's calculated total and elastic scattering cross-sections with the reference experimental data.

Nuclear reaction cross-sections were calculated using the recently released Empire code [7]. This code consists of several modules. The direct capture model was inserted to enhance the capture cross-section calculation. The width fluctuation correction influences the capture and inelastic scattering cross-sections. The calculated cross-sections are graphically compared with the experimental data and the evaluated files (ENDF/B-VI, JENDL-3.2, JEF-2.2, BRO-ND-2 and CENDL-2). The evaluated results are compiled to ENDF-6 format and they are merged with the evaluations in the resonance energy region to create a full data file. The general rules for merging with the resonance have also been established. The new files are in the preliminary stage for ENDF/B-VII adoption.

2. NUCLEAR MODELS

2.1 Optical Model Potential

The potential form was introduced and the corresponding parameters, as a function of the incident neutron energy, were established in a spherical optical model based on the reference experimental data. The Woods-Saxon well is used for the real part potential:

$$V_{(r)} = \frac{V}{1+\exp\left(\frac{r-R_v}{a_v}\right)} \quad (1)$$

where V and a_v are the strength and diffuseness of the potential, respectively. The nuclear radius R_v, related to the mass number A, is given by

$$R_v = r_v A^{1/3} \quad (2)$$

where r_v is the parameter to be searched. For the imaginary part potential, the derivative Woods-Saxon shape is used,

$$W(r) = \frac{4W \exp\left(\frac{r-R_w}{a_w}\right)}{\{1+\exp\left(\frac{r-R_w}{a_w}\right)\}^2} \quad (3)$$

where W, R_w, and a_w are the potential strength, radius, and diffuseness, respectively. The radius, R_w, is express as given in equation (2). Generally, the Thomas form is used in the optical model potential for the spin-orbit coupling:

$$V_{s\text{-}o}(r) = (2L*S)V_{so}\left(\frac{2}{r}\right)\frac{d\left(\frac{1}{1+\exp\left(\frac{r-R_{so}}{a_{so}}\right)}\right)}{dr} \quad (4)$$

where L*S is the dot product of the orbital and spin angular momentum operator.

The real and imaginary potential strength and radius are expanded as a function of the incident neutron energy:

$$V = Vo + V1 \cdot En, \quad rv = ro + r1 \cdot En, \quad (5a)$$
$$W = Wo + W1 \cdot En, \quad rw = rwo + rw1 \cdot En, \quad (5b)$$

where En is the incident neutron energy. The potential parameters (V_o, V_1, W_o, W_1, r_o, r_1, r_{wo}, r_{w1}, a_v, a_w, V_{so}, r_{so}, a_{so}) were established simultaneously. The determined potential produces the basic information (transmission coefficients) for the reaction calculation.

2.2 Reaction Models

Empire [7] is a modularized code system. The main utilities include masses, level densities and discrete levels, decay schemes, deformation parameters, γ-ray strength functions, Reference Input Parameter Library (RIPL), and ENDF-6 formatting and plotting capabilities. The main modules are: Optical model, Multi-step Direct and compound, Pre-equilibrium exiton (DEGAS) and Monte Carlo hybrid simulation (HMS), and a full featured Hauser-Feshbach including a width fluctuation correction.

The emission of neutrons, protons, α-particles, and light ions are taken into account along with the competing fission channel. In the statistical model of nuclear reactions, the Compound Nucleus (CN) state a with spin J, parity π, and excitation energy E to a channel b is given by the ratio of the channel width Γ_b to the total width $\Gamma_{tot} = \sum_c \Gamma_c$ multiplied by the population of this state $\sigma_b(E,J,\pi)$. This also holds for the secondary compound nuclei that are formed due to subsequent emissions of particles. Each such state contributes to the cross-section.

$$\sigma_b(E,J,\pi) = \sigma_a(E,J,\pi)\frac{\Gamma_b(E,J,\pi)}{\sum_c \Gamma_b(E,J,\pi)} \quad (6)$$

These have to be summed over spin J and parity π and integrated over the excitation energy E (in the case of daughter CN) to obtain the observable cross-sections. The particle decay width is given by

$$\Gamma_c(E,J,\pi) = \frac{1}{2\pi\rho_{CN}(E,J,\pi)}\sum_{J'=0}^{\infty}\sum_{\pi'}\sum_{j=J'-J}^{J+J'}\int_0^{E-B_c}$$
$$\rho_c(E',J',\pi')T_c^{l,j}(E-B_c-E')dE' \quad (7)$$

where Bc is the binding energy of particle c in the compound nucleus, ρ is the leveldensity,and $T_c^{l,j}(\varepsilon)$ stands for the transmission coefficient for particle c having a channel energy of $\varepsilon = E - B_c - E'$ and an orbital angular momentum l, which together with the particle

spin s couples to the channel angular momentum j. For the discrete levels, the level density $\rho(E, J^{\pi})$ reduces to $\delta(E-E_i)\delta_{(J^{\pi},J_i)}\delta_{(\pi^{\pi},\pi_i)}$.

Particular attention[7] has been dedicated to the determination of the level densities, which can be calculated via the non- adiabatical approach allowing for the rotational and vibrational enhancements. Level densities acquire dynamic features through the dependency of the rotational enhancement on the shape of a nucleus. The dynamic approach in Empire takes into account the collective enhancements of the level densities due to nuclear vibration and rotation. The level density is corrected for the rotational and vibrational collective effects in the non-adiabatic mode.

3. MERGE WITH RESONANCE

The evaluated results for the fast energy region were finally merged with the resonance (already adopted in ENDF/B-VI release 8) in an unresolved energy region, generally at the 1st excited energy level corresponding to a few keV or to several hundreds of keV of energy where the inelastic scattering reaction channel opens. From the different model calculations at the resonance and the fast energy, a discontinuity may occur at the merging energy. Therefore, where necessary, background and adjustments were added based on the experimental data. After merging, the NJOY [8] code was run to check the continuity and the file processing for applications. A general information file (MF1) was completed for each nucleus, including an evaluated file history, resonance evaluation, fast region information (OMP, levels, codes, parameters) and each reaction's description. Also, the general rules for the merge were established.

The general rules for merging are: For a total cross-section, with experimental data, continuity is considered from an agreement with the reference experimental data. On the other hand, without experimental data, experimental data for natural elements is considered instead. For a capture cross-section, without experimental data, the continuity and average cross-section value between the two different evaluations are considered at the merging region. With experimental data, the continuity is considered at the merge phase. An elastic scattering cross-section is created from the sum rule.

4. RESULTS AND DISCUSSIONS

The calculations were performed as follows. The established potential parameters are summarized in Table I. The selected energy dependent potential was applied in the whole fast energy region. SCAT2 included in Empire was used with the neutron parameters to produce the transmission coefficients. The discrete levels were then matched with the continuum. Afterwards, all the other input parameters for Empire were prepared. The calculated cross-sections are graphically compared with the experimental data and evaluated files for all the reaction channels. If the evaluation is satisfied, the calculated cross-sections are formatted in ENDF-6 and the results are combined with the resonance part. Otherwise, tuning of the parameters is necessary. By adding general information (MF1), the formatted file undergoesa physics checking using CHECKR, FIZCON, and PSYCHE. Fig. 1 shows the evaluation procedure.

The current evaluation and the merged data are nominated as ENDF/B-VII in the figure. Pd-105 does not have the experimental data for the total cross-section. Therefore, the natural element experimental data were used in the optical model potential parameter search. Fig. 2 shows a comparison of the calculated cross-section with the experimental data and the evaluated files. The new data shows a smooth connection with the resonance and agrees well with the natural experimental data [9]. ENDF /B-VI has an abnormal peak at 283.2 keV and the value is higher than the calculation and the experimental data at around 200 keV. Fig. 3 is the elastic scattering cross-section. There is no experimental data. Fig. 4 is the inelastic scattering cross-section. BROND has a different shape from the other evaluation files and it has a very high value above 10 MeV. Fig. 5 shows the capture cross -section. The calculation and the evaluated files are in good agreement with the experimental data [10,11]. The calculation shows a smooth connection between the fast energy and the resonance regions. Fig. 6 is the (n, p) cross-section. All the experimental data is around 14.5 MeV. All the evaluated files agree well at 14.5 MeV[12]. However, at the low energy region, each evaluation has a different shape. The referenced measured data and the merged energies are summarized in Table II.

The total cross-section on Ag-109 is shown in Fig. 7. The experimental data does not exist for the total, and therefore, the natural element experimental data is used. The calculation and ENDF/B-VI agree well with the natural experimental data [13]. Fig. 8 is the elastic scattering cross-section. The difference is displayed until 100 keV between the calculation and the ENDF/B-VI. Fig. 9 is the inelastic scattering cross-section. The calculation and the ENDF/B-VI agree well with the experimental data [14] in the higher energy region. Fig. 10 shows the capture cross-section. The calculation and the ENDF/B-VI agree well with the experimental data [15]. However, the calculation shows a direct capture feature in the pre-equilibrium region whereas this feature is not found in the ENDF/B-VI. Fig. 11 is the (n, p) cross-section. The calculation agrees well with the reference experimental data [16].

Xe-131 does not have experimental data for the total cross-section either. Therefore, the natural element experimental data was used in determining the potential

Table 1. Searched potential parameters

Parameter	Pd-105	Ag-109	Xe-131	Cs-133
Vo	48.51	48.25	45.27	46.00
V1	-0.5528	-0.30	-0.199	-0.25
ro	1.265	1.249	1.305	1.277
av	0.520	0.463	0.620	0.62
Wo	7.9653	7.701	7.702	7.00
rwo	1.339	1.299	1.247	1.3750
aw	0.440	0.635	0.550	0.35
Vso	5.261	6.000	7.000	7.00
rso	1.265	1.249	1.277	1.277
as	0.2670	0.603	0.620	0.620
W1	-0.053	-0.150	0.000	0.000
rw1	0.000	0.000	0.000	0.000
r1	0.000	0.000	0.000	0.000

Table 2. Reference experimental data and energy for the merge with the resonance

Nuclide	Reference experimental data		Merging energy (keV)
	Total	Capture	
Pd-105	83Poenitz[9]	82Cornelis, 79Macklin[10,11]	283.21
Ag-109	95Litvinskiy, 83Poenitz[9,13]	87Bokhovko[15]	81.162
Xe-131	60Vaughn[17]	-	73.895
Cs-133	71Foster Jr.[19]	91Bokhovko[20]	73.844

parameters. Fig. 12 shows a comparison of the calculation with the experimental data and ENDF/B-VI. ENDF /B-VI does not agree well with the experimental data [17] between 80 keV and 250 keV. Fig. 13 is the elastic scattering cross-section. The calculation shows a strong difference from ENDF/B-VI from 5 keV to 400 keV. Fig. 14 is the inelastic scattering cross-section. There is no experimental data for the inelastic scattering cross-section. Fig. 15 is the capture cross-section. The calculation shows the fast neutron capture prominently in the pre-equilibrium. On the other hand, ENDF/B-VI decreases continuously after 6 MeV. Fig. 16 is the (n, p) cross-section. The evaluated files agree with the experimental data [18] at around 14 MeV.

Fig. 17 is the total cross-section for Cs-133. The calculation shows a smooth connection with the resonance and agrees well with the experimental data [19]. Though ENDF/B-VI has a different shape in the measured range from the calculation, it displays good agreement with the experimental data and is within the fluctuation error. Fig. 18 is the elastic scattering cross-section. The calculation shows a significant difference from ENDF/B-VI from 4 keV to 500 keV. Fig. 19 is the inelastic scattering cross-section. There is no experimental data. Fig. 20 shows the capture cross-section for the calculation and the evaluated files. The calculation and the ENDF/B-VI agree well with the experimental data [20]. Fig. 21 is for the (n, p) cross section. The calculation and ENDF/B-VI are in good agreement with the experimental data [21] at 14.5 MeV, but the shape between the calculation and the ENDF/B-VI is somewhat different. ENDF/B-VI has an abnormal peak at 5 MeV. While only selected results are presented here, the other threshold reaction cross-sections are also calculated and evaluated. The final file involves MF3, MF4, MF6, MF12, and MF14.

5. CONCLUSION

The selected energy dependent optical model potential, based on the experimental data, was suitable for producing the model calculated cross-sections in the energy range above the resonance region. The total and capture cross-sections were connected with the resonance smoothly and continuously in the unresolved energy

region. If necessary, due to the two different energy regions and evaluations, background was added in the unresolved resonance region. The merge rules setup was applicable and will be used as a standard for other nuclei evaluation.

Empire was successful in producing the reaction cross-sections. The total, capture, and other threshold calculated cross-sections are in good agreement with the experimental data. They represent a substantial improvement over the current ENDF/B-VI. The results were converted into ENDF-6 format. At the pre-equilibrium energy region, the calculated capture cross-section prominently shows the fast neutron direct capture phenomena.

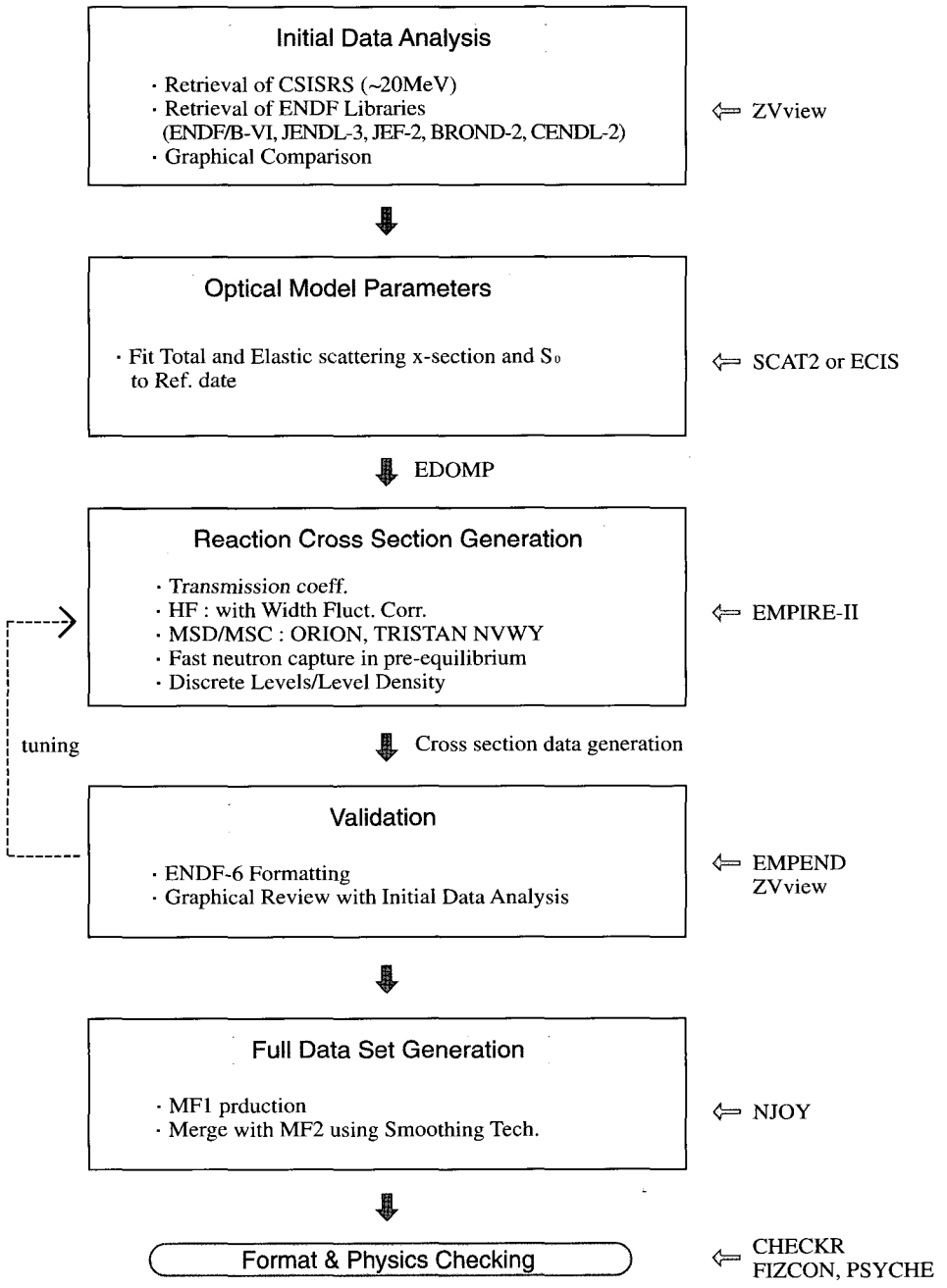

Fig. 1. Process of theoretical model calculation and evaluation.

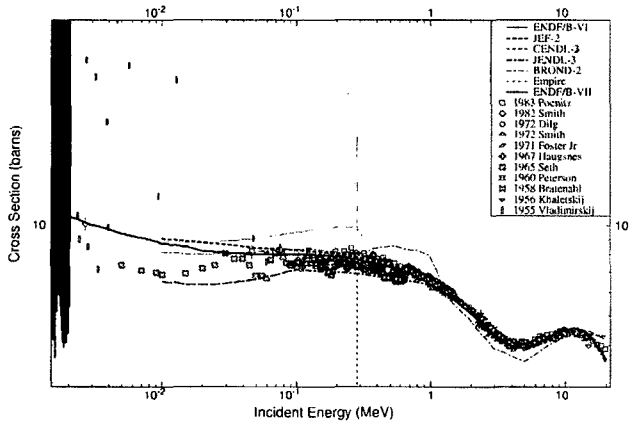

Fig. 2. Total cross section of Pd-105.

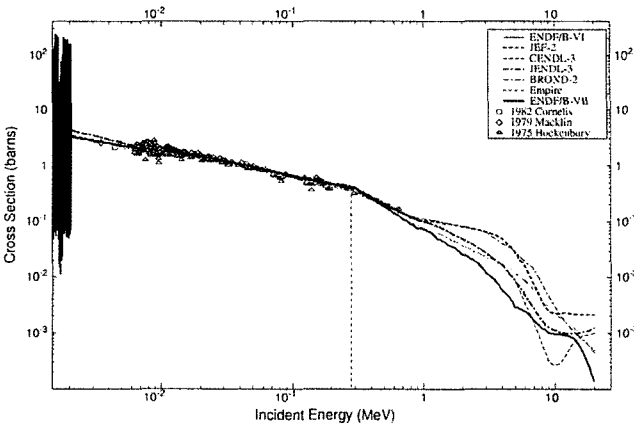

Fig. 5. (n, γ) cross section of Pd-105.

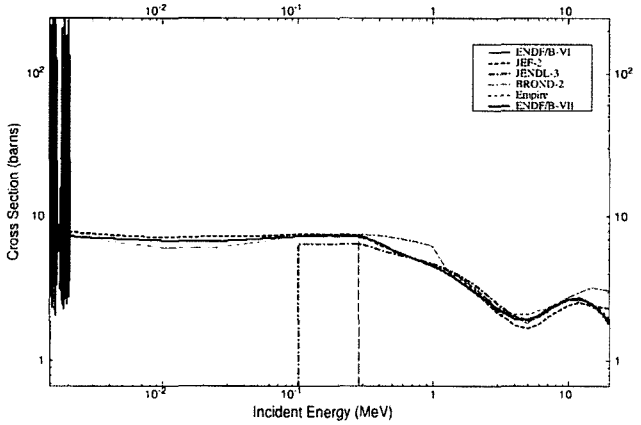

Fig. 3. (n, n) cross section of Pd-105.

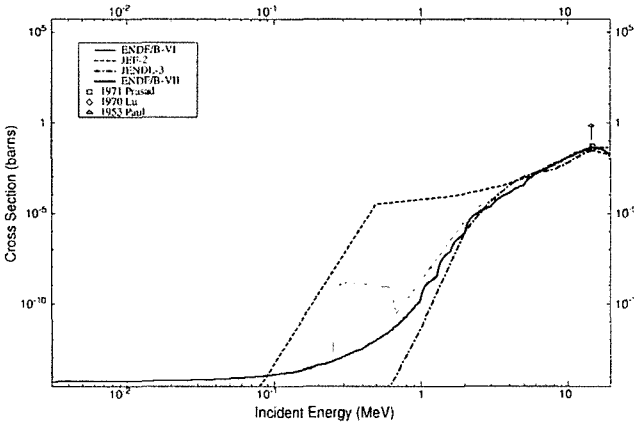

Fig. 6. (n, p) cross section of Pd-105.

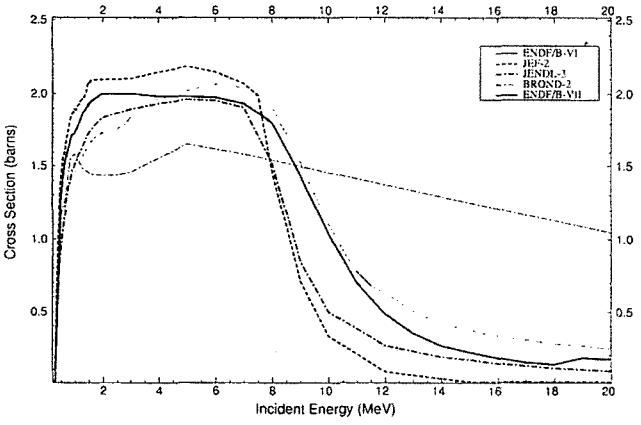

Fig. 4. (n, n') cross section of Pd-105.

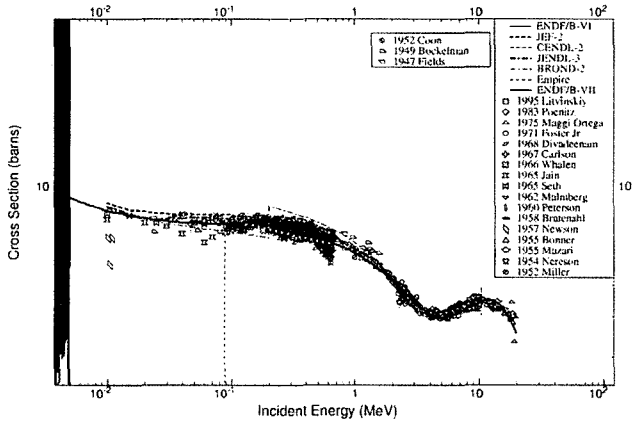

Fig. 7. Total cress section of Ag-109.

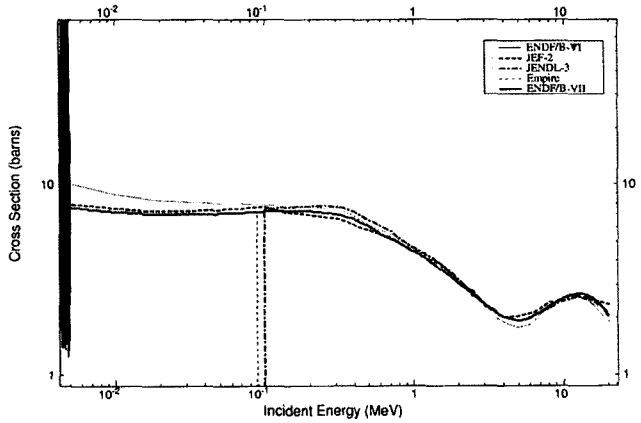

Fig. 8. (n, n) cross section of Ag-109.

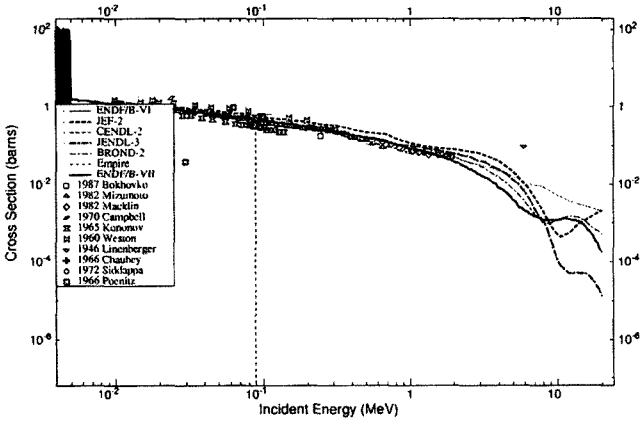

Fig. 10. (n, γ) cross section of Ag-109.

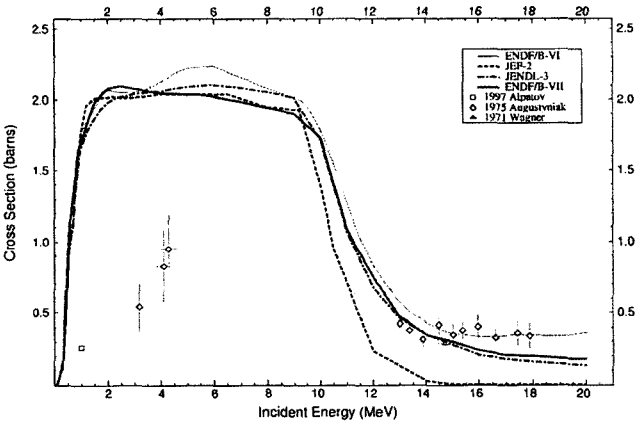

Fig. 9. (n, n') cross section of Ag-109.

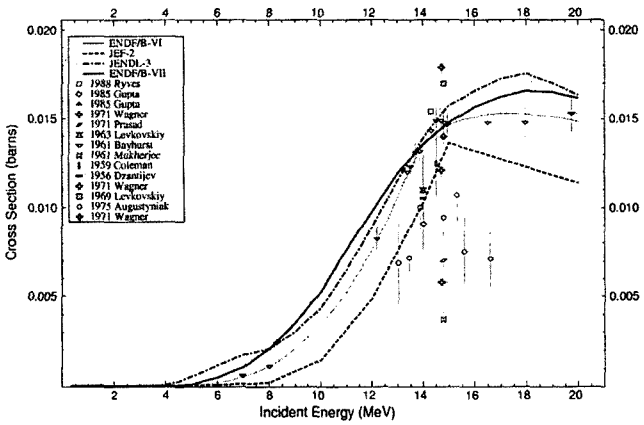

Fig. 11. (n, p) cross section of Ag-109.

Acknowledgement

This work has been performed under the auspices of the Korea Ministry of Science and Technology as a long-term R&D project.

REFERENCES

[1] Y.D. Lee and J.H. Chang, "Neutron Cross Section Evaluation on Pr-141, Nd-143 Nd-145, Sm-147 and Sm-149," J, KNS, 34, 4, 370, 2002.

[2] Y.D. Lee and J.H. Chang, "Neutron Cross Section Evaluation on Mo-95, Tc-99 Ru-101 and Rh-103 in the Fast Energy Region," J, KNS, 34, 6, 533, 2002.

[3] S.Y.Oh and J.H.Chang, Neutron Cross Section Evaluations of Fission Products below the Fast Energy Region, BNL-NCS-67469 (KAERI/TR-1511/2000), Brookhaven Natoinal Laboratory.

[4] E.D. Arthur and P.G. Young, Symp. on Neutron Cross Sections from 10 to 50 MeV, Upton, May 1980, Brookhaven report BNL-NCS-51245 (1980). p. 731.

[5] Y. D. Lee, ABRXPL development for parameter decision of spherical optical model potential, KAERI, NDL-14/99.

[6] R.D.Lawson, ABAREX_A Neutron Spherical Optical-Statistical Model Code, in Workshop on Computation and Analysis of Nuclear Data Relevant to Nuclear Energy and Safety, pp447, Trieste, Italy.

[7] M.Herman, Empire-2: Statistical Model Code for Nuclear Reaction Calculations, IAEA, Vienna.

[8] R.E. MacFarlane, D.W. Muir, The NJOY Nuclear Data Processing System, Version 91, LA-12740-M, Oct., 1994.

[9] P. Poenitz, J.F. Whalen, "Neutron Total Cross Section Measurements in the Energy Region from 47 keV to 20 MeV," R, ANL-NDM-80, 1983.

[10] L. Macklin, J. Halperin, R.R. Winters, "Pd-104,105,106, 108,110 (n, γ) Cross Sections above 2.6-KeV," J, Nucl. Sci. Eng., 71, 182, 1979.

[11] E. Cornelis et al., "Average Capture Cross Section of The Fission Product Nuclei Pd-104 Pd-105 Pd-106 Pd-108 Pd-

110," C, 82ANTWER, 222, 1982.
[12] R. Prasad, D.C. Sarkar, "Measured (n, p) Reaction Cross-Sections and Their Predicted Values at 14.8 MeV," J, NC/A, 3, (3), 467, 1971.
[13] L. L. Litvinskiy et al., "Neutron Inelastic Cross-Section on Silver at The Energy 275 KeV," J, YK, (4), 38, 950, 1994.
[14] W. Augustyniak et al., "Cross Sections for The Inelastic Scattering, (n, p) and (n, 2n) Reactions on Ag-107 and Ag-109 Isotopes," J, NP/A, 247, 231, 1975.
[15] M. V. Bokhovko, "Neutron Radiative Capture Measurements in Silver in The Energy Range 4-400 keV," J, YK, (2), 21, 1987.
[16] J.P. Gupta et al., "Pre-equilibrium Emission Effect in (N,P) Reaction Cross Section at 14.8 MeV," J, PRM, 24, 637, 1985.
[17] F. J. Vaughn et al., "Total Neutron Cross Sections of Helium, Neon, Argon, Krypton and Xenon," J, PR, 118, 683, 1960.
[18] R.A. Sigg, P.K. Kuroda, "14.6-MeV Neutron Activation Cross Sections for The Xenon Isotopes," J, NSE, 60, 235, 1976.
[19] D.G. Foster JR, D.W. Glasgow, "Neutron Total Cross Sections, 2.5 - 15 MeV," J, PR/C, 3, 576, 1971.
[20] M. V. Bokhovko et al., "Neutron Radiation Cross-Section, Neutron Transmission And Average Resonance Parameters For Some Fission Product Nuclei," R,FEI-2168-91,1991.
[21] S.M. Qaim, "Activation Cross-Sections for Some 14.8 MeV Neutron Induced Nuclear Reactions on Caesium, Isomer Ratio of CS-133, XE-133 and I-130," J, JIN, 32, 1799, 1970.